JOURNAL OF NANO- AND ELECTRONIC PHYSICS
Vol. **9** No 3, 03041(4pp) (2017)

ЖУРНАЛ НАНО- ТА ЕЛЕКТРОННОЇ ФІЗИКИ
Том **9** № 3, 03041(4cc) (2017)

PbS-ZnO Solar Cell: A Numerical Simulation

Jaymin Ray[1,*], Tapas K. Chaudhuri[2], Chetan Panchal[3], Kinjal Patel[1], Keyur Patel[4], Gopal Bhatt[4], Priya Suryavanshi[3]

[1] *Department of Physics, Uka Tarsadiya University, Bardoli, Dist. Surat, Guajrat 394120, India*
[2] *Department of Physics, SVNIT, Surat, Gujarat 395007, India*
[3] *Applied Physics Department, M.S. University of Baroda, Vadodara, Gujarat 390001, India*
[4] *Science and Humanity Department, BITS Education Campus, Vadodara, Gujarat 390001, India*

(Received 28 April 2017; revised manuscript received 10 May 2017; published online 30 June 2017)

Nanoscale PbS, especially quantum dots (QDs) are of interest in applications, such as, solar cells and photodetectors because of tunability of band gap from 0.5 to 3 eV. Recently, ZnO/PbS solar cells with 8.55 % conversion efficiency have been reported with films made deposited from ligand exchanged PbS QDs. However, nanocrystalline PbS is easier to fabricate than QDs. This paper reports theoretical investigation into the use of nanocrystalline PbS in place of QDs as solar cell absorber. Solar cells with a structure of SLG/ITO/ZnO or CdS/PbS/Al was simulated using SCAPS software. We have used two n-type materials one is ZnO and second is CdS. The comparative simulated device performance was studied by current-voltage (*I-V*) characteristics and quantum efficiency (QE). The final results reveal a power conversion efficiency of 18.5 % for solar cells with *p*-PbS as absorber and *n*-ZnO as buffer and 16.8 % for *n*-CdS buffer layer.

Keywords: PbS Thin Film, Numerical Simulation, Current-Voltage characteristic, QE analysis.

DOI: 10.21272/jnep.9(3).03041 PACS numbers: 78.20.Bh, 73.40.Lq, 84.60.Jt

1. INTRODUCTION

During the last decades various promising solar-cell concepts, ranging from single-crystal silicon, through thin-film technologies to purely organic devices, had been developed and demonstrated intensively. Looking to the present state of art for the large-scale implementation of solar cell, the cost, efficiency, reliability, and potential has to taken in to account. The use of solution processed earth abundant inorganic material in the fabrication of solar cell is a new and promising route for cost efficient, reliable and flexible device structures [1, 2]. Recent development on solution-processed inorganic solar cells (CZTS and CIGS) and colloidal quantum-dot (CQD) solar cells clearly stated better performance and stability compare to organic solar cell and DSSC. Solution-synthesized and processed semiconduc¬tor nanocrystals, viz. QDs, solar cells based on the PbS has shown a promising future with merits of low-cost processing, tunable spectral absorption, long-lifetime hot carriers, and multiple exciton generation by a single photon [3, 4]. That offers a line of approach to make a tandem and multi-junction solar cells, which make excellent use of the dispersion of solar spectrum. Progress in the materials, its chemistry and engineering for charge-extraction from the solar cell through respective electric contact has recently produced significant improvements in nanocrystals photovoltaics.

A very first approach on the nanocrystal based solar cell device was a Schottky structure of Lead Sulphide (PbS) CQDs sandwich between the transparent conductive oxide and a shallow-work-function metal [5]. The benefit of these devices was its ease of fabrication that leads advancement in the CQDs photovoltaic. With that some limitations were observed like Fermi level pinning at the CQD/metal interface, that limits the open-circuit voltage, less efficient charge separation and backward recombination due to the small barrier for hole injection at the electron-extracting electrode. To address these limitations a depleted-heterojunction having a n-type wide-bandgap semiconductors such as TiO_2 [6], ZnO [7], and CdS [8] that form a rectifying junction with a *p*-type CQD film was developed in 2010. Recently, a new record performance of 8.5 % was reported for the structure ITO/ZnO/QDPbS-TBAI/QDPbS-EDT/MoO_3/Au/Ag [9].

The chemical synthesis of PbS QDs are basically complicated, multi-stepped and time consuming. To restrain the growth of PbS QDs often requires capping agents which act as an insulating layer impeding the transport of electrons. However, solar cell or any device made from PbS QDs would necessitate the deposition of thin films by any direct coating techniques. For deposition of films, capping layer on PbS QDs has to be removed and then dispersed in another solvent. Thus, deposition of PbS QD films has not only consists of number of steps and also time consuming. Hence, a direct deposition process which will yield nanoscale PbS films in one step would be very useful for the development of nano PbS solar cells. It has been found that nanocrystalline PbS films having bang gap of 1.4 eV can be easily deposited by one-step direct deposition technique. Such

* jayminray@gmail.com

nanocrystalline PbS films can now be used to fabricate PbS/ZnO thin film solar cells. In this paper we explore theoretically thin film solar cells based on nanocrystalline PbS films. Then experimentally investigate a proof-of-concept all-solution PbS/ZnO solar cell.

2. NUMETICAL MODELING

Numerical simulations can be used to provide insight to interpret measurements and to assess the potential of a cell structure. The simulations can be used to analyse the effect of the variation of material parameters, to obtain the optimal values for optimizing the solar cells efficiencies. In the case of PbS QD solar cell highest efficiency was observed with n-ZnO layer. On the other hand *n*-CdS also had potential for the n-layer. In concern with that in this work, we simulate and compare the performance solar cell by varying the *n*-type layer viz. ZnO and CdS.

2.1 Device Structure

A numerical simulation package SCAPS-1D was used for modeling the PbS solar cell structure, shown in Fig. 1 and 2 (simulation screen shot). It can calculate the steady-state band diagram, the carrier transport in one dimension, the recombination behavior based on the Poisson equations [10], and the hole and electron continuity equations.

$$\frac{d^2}{dx^2}\Psi(x)=\frac{e}{\varepsilon_0\varepsilon_r}\left(p(x)-n(x)+N_D-N_A+\rho_p-\rho_n\right), \quad (1)$$

where, Ψ is electrostatic potential, e is electrical charge, ε_r is relative and ε_0 is the vacuum permittivity, p and n are hole and electron concentrations, N_D is charged impurities of donor and N_A is acceptor type, ρ_p and ρ_n are holes and electrons distribution, respectively. The continuity equations for electrons and holes are,

$$\frac{d}{dx^2}J_n(x)-e\frac{\partial n(x)}{\partial t}-e\frac{\partial \rho_n}{\partial t}=G(x)-\mathrm{R}(x), \quad (2)$$

$$\frac{d}{dx^2}J_p(x)+e\frac{\partial p(x)}{\partial t}+e\frac{\partial \rho_n}{\partial t}=G(x)-\mathrm{R}(x), \quad (3)$$

where J_n and J_p are electron and hole current densities, $G(x)$ and $R(x)$ are charge generation and recombination rates. The optical charge generation (G_{op}) is describe by the following expression,

$$G_{op}(x)=-\frac{d}{dx}\sum_i\Phi_i^{FOR}(\lambda_i)+\frac{d}{dx}\sum_i\Phi_i^{REV}(\lambda_i), \quad (4)$$

where $\Phi_i^{FOR}(\lambda_i)$ and $\Phi_i^{REV}(\lambda_i)$ are, respectively, the photon flux of the incident light and the light reflected from the back surface at a wavelength of λ_i at some point x, depending on the light absorption coefficient, and the light reflectance in the forward and reverse direction. In our simulation, the reflection indices for the forward (R_F) and reverse (R_B) directions are 0 and 0.6, respectively. The term $R(x)$ in Eqs. (2) and (3) is the recombination rate of photo-generated carriers.

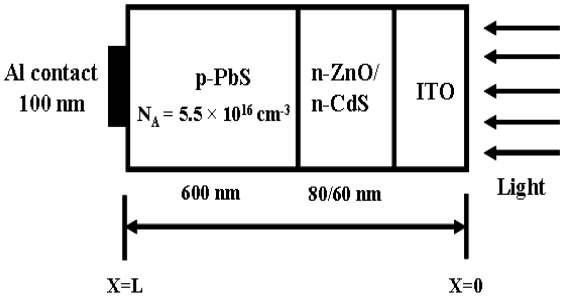

Fig. 1 – Schematic of PbS solar cell structure used for the simulation

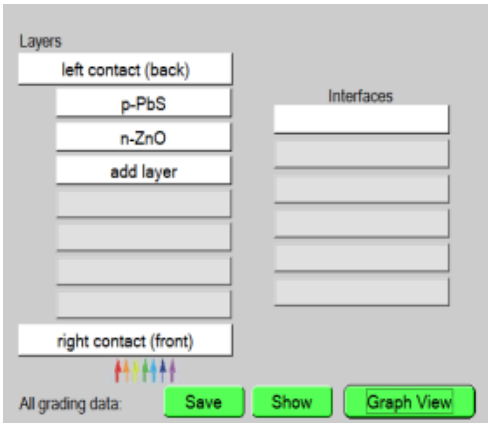

a

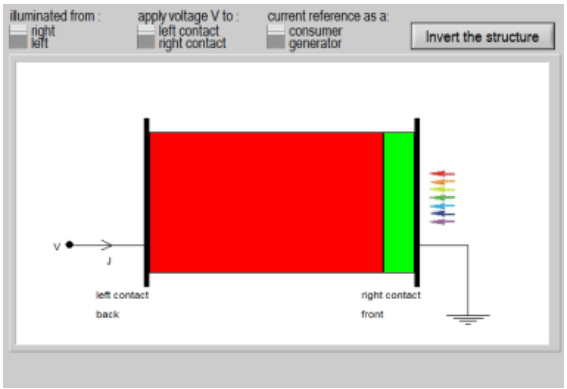

b

Fig. 2 – Schreenshot of the device structure defination (a) and the shmetic of the structure (b) used in SCAPS

In SCAPS program, the interface states, which act as a recombination centre, can be distributed in energy states, in the same way as the bulk states. At the metal–semiconductor interfaces (contacts), surface recombination velocity S_n or S_p describe the transport of minority carriers and the thermionic emission [11] describe the transport of majority carriers. In SCAPS, at interfaces between the layers or at contacts the tunneling is not implemented.

To define the whole device at every point of x, one should determine $\Psi(x)$, *n*-type quasi-Fermi level (E_{Fn}), and the p-type quasi-Fermi level (E_{Fp}), $n(x)$, and $p(x)$. Because the non-linear behavior of $\Psi(x)$, E_{Fn}, and E_{Fp} equation, cannot be solved analytically without setting any boundary conditions. The Newton-Raphson tech-

nique is used in the SCAPS-1D to solve these equations by applying some boundary conditions [12].

2.2 Materials and Optical Parameters

The material parameters used for the simulation is tabulated in Table 1. In addition to that a screen shot of material parameter is shown in Fig. 3. A light trapping structure was not considered in the simulation. The contact between the film and the electrode is ohmic. The simulated light is AM 1.5, and its effective wave band is in the range of 0.3-0.9 μm.

Table 1 – Parameters used for the PbS solar cell simulation

Parameters	*p*-PbS	*n*-ZnO	*n*-CdS
Thickness (nm)	600	80	60
Band gap (eV)	1.4	3.4	2.4
Electron affinity, χ (eV)	4.35	4.55	4.45
CB density of states, N_c (cm^{-3})	$2 \cdot 10^{18}$	$4 \cdot 10^{18}$	$2 \cdot 10^{18}$
VB density of states, N_v (cm^{-3})	$2 \cdot 10^{18}$	$9 \cdot 10^{18}$	$1.5 \cdot 10^{18}$
Hole mobility, μ_h (cm^2/Vs)	20	20	20
Electron mobility, μ_e (cm^2/Vs)	50	50	50
Donor density, N_D (cm^{-3})	$1 \cdot 10^{1}$	$5 \cdot 10^{20}$	$1 \cdot 10^{19}$
Accepted density, N_A (cm^{-3})	$5.5 \cdot 10^{16}$	$1 \cdot 10^{1}$	$1 \cdot 10^{1}$

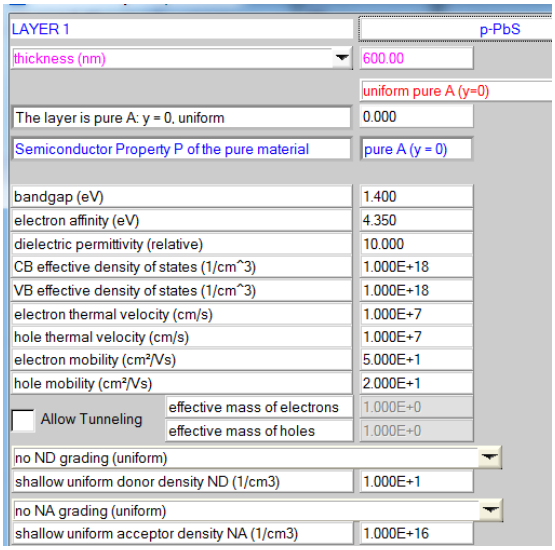

Fig. 3 – Layer properties panel of SCAPS

In the present case we had consider the zero tunneling of electrons in the illumination condition. In addition to that we had se the uniform grading of accepter and donor density.

The optical absorption constant can be set from either from a model or from an experimental data file. In the present work we have used the experimental optical data for PbS and ZnO films.

The band gap values of PbS and ZnO are 1.4 eV and 3.5 eV respectively. In addition to that the absorption coefficient, α, is $10^5\ cm^{-1}$ and $10^1\ cm^{-1}$ for PbS and ZnO films respectively in the Visible region. One can calculate, $\alpha(\lambda)$ using the relation (Eq. 5),

$$\alpha(\lambda) = \left(A + \frac{B}{h\nu}\right)\sqrt{h\nu - E_g}, \qquad (5)$$

where α = absorption coefficient, E_g = Energy band gap, $h\nu$ = Photon energy, A and B = Wavelength dependent absorption constant.

2.3 Contact Properties

In order to define any optoelectronics structure, the properties of contact plays vital role in the efficient performance of a device. In the present PbS/ZnO Solar cell structure we have used graphite as a top contact and the ITO used as a back contact. In the latest version (after 1/1/2014) instated of simplified algorithm for any n-type, p-type of intrinsic type, the "flat bands" calculation is provided, and used to provide The metal work function Φ_m (for majority carriers). In the Flat bands case, SCAPS calculates for every temperature the metal work function, Φ_m, in such a way that flat band conditions prevail. In addition to that the (wavelength dependent) reflection/transmission values at the contacts should be set accordingly.

3. RESULTS AND DISCUSSION

The resulting *J-V* characteristic of PbS solar cell, as shown in Fig. 4, with two different n-type material viz. *n*-ZnO and *n*-CdS. In both case it can be clearly observed that nearly equal open circuit voltage (V_{oc}) values and a minor difference (about 2 mA/cm^2) in short circuit current density (J_{sc}) values.

The major difference is observed in the Fill Factor Values i.e. 0.82 in the case of *n*-ZnO and 0.76 in the

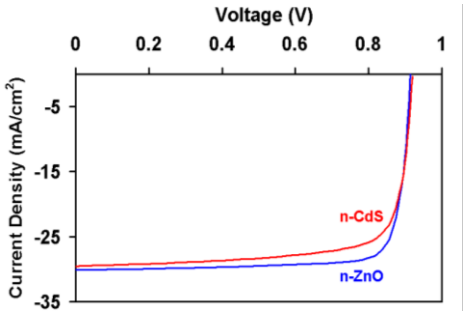

Fig. 4 – *J-V* characteristic variation of PbS solar cell with two different *n*-type material, i.e. n-ZnO and *n*-CdS

n-CdS. That affects the overall performance of the solar cell device. PbS solar cell having a *n*-ZnO shows the conversion efficiency of about 18.5 %, while in the case of *n*-CdS it is 16.8 %. The values of *J-V* parameters are shown in Table 2.

Table 2 – Extracted J-V parameter of PbS solar cell

Parameters	*n*-ZnO	*n*-CdS
V_{OC} (V)	0.90	0.91
J_{SC} (mA/cm^2)	30.14	28.91
FF	0.82	0.76
η	18.5	16.8

The difference in the values of conversion efficiency can be explained in terms of the difference between the valance bands (ΔE_v). In a simple diode, current can be said when hole of *p*-type transport to *n*-type. This indicates there is a possibility of recombination near or a middle of the junction, even in the most ideal device. So

there is a need to specify recombination somewhere, at least at one place. In the bulk of a semiconductor layer, generally three different types of recombination processes: through defects, radiative and Auger. In case of the SCAPS simulation we had taken the "neutral" defect, is an idealization to which contributes to the Shockley-Read-Hall recombination but does not contribute to the space charge. The "neutral" defect, only the product of σ and N_t affects the *dc* and *ac* solutions, through the carrier lifetimes; τ_n e.g. is given by $1/(\sigma_n N_t V_{th})$. In a simple word we can say that, a neutral defect does not exist in reality, but it's idealization helps to create a model [13].

From the Fig. 5 we can clearly see that the value of ΔE_v is higher in case of n-ZnO compare to the *n*-CdS structure. The higher the ΔE_v, in general, prevent the electron hole pair recombination at the interface. In these regards we observed the higher conversion efficiency in case of PbS/ZnO structute i.e. 18.5 %. In case of PbS/CdS structure it was 16.8 %.

Looking towards the spectrum response (Fig. 6), *QE* curves of these two cells, in 520-900 nm region the response of both solar cell is almost identical. The cut-off of *QE* at 890 nm corresponds to the PbS band gap. In 300-520 nm region the noticeable difference is observed in *QE* value. Below 520 nm, *QE* values starts decreasing in the case of PbS solar cell having a *n*-CdS. That indicates band gap of CdS which stats absorbing light of wavelength below 520 nm, i.e. blue and *UV* region. So, the wavelength below 520 nm cannot fully contribute in the generation of electron. In the case *n*-ZnO the *Q*E values starts decreasing below 360 nm, which indicates the whole visible region, contribute to

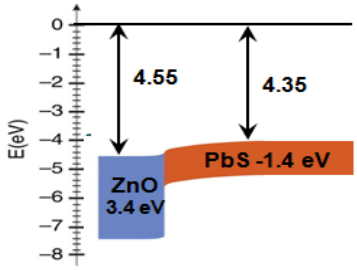

a

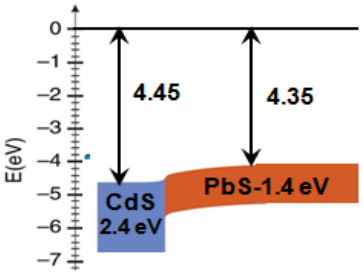

b

Fig. 5 – Band diagram of PbS/ZnO structure (a), and PbS/CdS structure

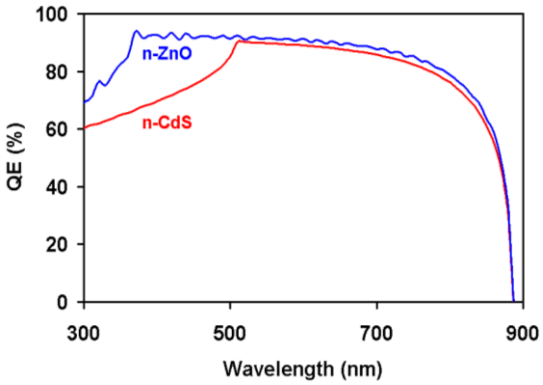

Fig. 6 – Variation of Spectral response of PbS solar cell in case of different n-type layer

generation of electrons. Because of these reason PbS Solar cell having a *n*-ZnO layer shows the higher fill factor and higher efficiency compare to the *n*-CdS layer.

4. CONCLUSION

Simulation shows the feasibility of PbS can be used for the fabrication of solar cell, and *n*-ZnO is the suitable partner compare to the CdS to form a pn junction. A simulation result shows 18.5% conversion efficiency and better *QE* response in case of PbS/ZnO solar cell.

REFERENCES

1. J. Tang, Sargent E. H. Infrared, *Adv. Mater.* **23**, 12 (2011).
2. Taesoo D. Lee, Abasifreke U. Ebong, *Renewable and Sustainable Energy Reviews*, **70**, 1286 (2017).
3. F.W. Wise., *Acc. Chem. Res.* **33**, 773 (2000).
4. M.V. Kovalenko, D.V. Talapin, M.A. Loi, F. Cordella, G. Hesser, M.I. Bodnarchuk, W. Heiss, *Angew. Chem. Int. Ed.* **47**, 3029 (2008).
5. R. Debnath, J. Tang, D.A. Barkhouse, X. Wang, A.G. Pattantyus-Abraham, L. Brzozowski, L. Levina, E.H. Sargent, *J. Am. Chem. Soc.* **132**, 5952 (2010).
6. A.G. Pattantyus-Abraham, I.J. Kramer, A.R. Barkhouse, X. Wang, G. Konstantatos, R. Debnath, L. Levina, I. Raabe, M.K. Nazeeruddin, M. Grätzel, E.H. Sargent, *ACS Nano.* **4**, 3374 (2010).
7. J.M. Luther, J. Gao, M.T. Lloyd, O.E. Semonin, M.C. Beard, A.J. Nozik, *Adv. Mater.* **22**, 3704 (2010).
8. L.-Y. Chang, R.R. Lunt, P.R. Brown, V. Bulović, M.G. Bawendi, *Nano Lett.* **13**, 994 (2013).
9. C.M. Chuang, P.R. Brown, V. Bulovic, M.G. Bawendi, *Nat. Mater.* **13**, 796 (2014).
10. S.M. Sze, K.Ng. Kwok., *Physics of semiconductor devices (3rd Edition)* (New York: A John Wiley & Sons, INC., Publication: 2007).
11. I. Repins, M. Contreras, M. Romero, Y. Yan, W. Metzger, J. Li, S. Johnston, E. Brian, C. DeHart, J. Scharf, *33rd IEEE Photo-voltaic Specialist Conference* (San Diego: California: 2008).
12. H. Movla, D. Salami, S. Sadreddini, *Appl. Phys. A* **109**, 497 (2012).
13. M. Burgelman, P. Nollet, S. Degrave, *Thin Solid Films* **361-362**, 527 (2000).